Research Article | Vol. 1, No. 1 | 15 Sep 2018 | OSA CONTINUUM 181

OSA CONTINUUM

Tunable fluidic lenses with high dioptric power

OSAMU TAKAYAMA,[1] FERNANDO MINOTTI,[2,3] AND GRACIANA PUENTES[2,4*]

[1] *Department of Photonics Engineering, Technical University of Denmark, Ørsteds Plads, Building 343, DK-2800 Kgs. Lyngby, Denmark*
[2] *Universidad de Buenos Aires, Facultad de Ciencias Exactas y Naturales, Departamento de Física, Buenos Aires, Argentina*
[3] *CONICET-Universidad de Buenos Aires, Instituto de Física del Plasma (INFIP), Buenos Aires, Argentina*
[4] *CONICET-Universidad de Buenos Aires, Instituto de Física de Buenos Aires (IFIBA), Buenos Aires, Argentina*
[*] *gracianapuentes@gmail.com*

Abstract: We report a complete theoretical model and supporting experimental results on the fabrication and characterization of macroscopic adaptive fluidic lenses with high dioptric power, tunable focal distance, and aperture shape. The lens is 17 mm wide and is made of an elastic polydimethylsiloxane (PDMS) polymer, which can adaptively restore accommodation distance within several cm according to the fluidic volume mechanically pumped in. Moreover, the lens can provide for magnification in the range of +25 diopter to +100 diopter with optical aberrations within a fraction of a wavelength, and overall lens weight of less than 2 g. The agreement between the non-linear theoretical model describing the elastic membrane deformation and the experimental results is apparent. We stress that these features make the proposed lenses appropriate for the low vision segment, as well as for applications in video magnifiers, camera zooms, telescope and microscopes objectives, and other machine vision applications where large magnification is required.

1. Introduction

National estimates reveal that the vision correction market in the U.S. nowadays is enormous. About seven out of ten Americans 18 years of age and older wear some type of corrective lens, a figure that jumps to 90% and higher among those 50 and older. Refractive errors are typically corrected by permanent means such as glasses, contact lenses or surgery. Standard eye-wear corrects for refractive errors by shifting the focal plane in the case of myopia and hyperopia, or by introducing astigmatic correction in the case of astigmatism and other higher-order aberrations [1–3]. Moreover, in many situations visual impairments are combined, for instance most myopia and hyperopia patients also suffer from presbyopia requiring multi-focal lenses. However, permanent multi-focal lenses limit the accommodation range of the eye and therefore limit the field-of-view to small focal regions suitable to observe an object at different distances, thus resulting in considerable vision loss [4]. Currently, visual impaired patients, such as the result of glaucoma or visual trauma, rely on organic glasses of large dioptric power. Large dioptric power with standard lenses can only be achieved with thick and heavy components, which introduce a large number of optical aberrations, making the glasses very bulky and unpractical. Moreover, the employed standard lenses are static and can only provide for a fixed focal distance.

To our knowledge, all previous prototypes for adaptive eye-wear [5–7] focus on different segments of the vision market, with moderate augmentation requirements. In particular, in Ref. [5] the author propose a fluidic lens prototype with optical power in the range (+/-6 D to +/-20D). On the other hand in Ref. [6], the authors propose a fluidic lens prototype with optical power in the range (+/-3D to +/-4 D). Here, we present the first macroscopic fluidic lens eyewear prototype with high dioptric power (+25D to +100D range) with optical aberrations below a

#335187 https://doi.org/10.1364/OSAC.1.000181
Journal © 2018 Received 14 Jun 2018; revised 17 Jul 2018; accepted 17 Jul 2018; published 12 Sep 2018

OSA CONTINUUM

fraction of the wavelength, which can adaptively restore accommodation distance within several cm, thus enabling access to the entire field-of-view. The lens is made of an elastic polymer which can adaptively modify its optical power according to the fluidic volume mechanically pumped in. Such liquid lens exhibits a large dynamic range, and its focusing properties are polarization independent [8]. Additionally, we demonstrate that by tuning the lens aperture it is possible to address different optical aberrations, thus providing an additional degree of freedom for the lens design. Our design is not only attractive for adaptive eye-wear, but also for camera, optical zooms, microscope objectives, and other machine vision applications where large magnification can be required [9]. We stress that, in contrast to other previous results reported in the literature [10, 11], our prototype presents not only reduced spherical aberrations, but also reduced aberrations of higher and lower order than spherical, such as trefoil, astigmatism, and coma.

Adaptive fluidic lenses can be classified in two main categories, according to their operation mechanism. The first class is the electro-wetting lens whose focal length can be tuned continuously by applying a controlled external voltage [12–14]. While the advantage of electro-wetting lenses is that they can provide for large focusing power with no mechanical moving parts, the disadvantage is a relatively high driving voltage required, in addition to limited stability and liquid evaporation. The second type is the mechanical lens, whose focal length is controlled by pumping liquid in and out of the lens chamber, which changes the curvature of the lens profile [15–22]. The adaptive lenses reported here belong to the second category. For this demonstration of principle, we pump the fluid in by using a syringe pump. We note that the mechanical pump itself is not the focus of this report.

Our original contribution consists of a fully developed theoretical model for the elastic membrane, not previously presented and which is fully confirmed by experimental results. We also provide a thorough study of lens aberrations, at a magnification scale and dynamic range not previously studied. The article is organized as follows: In Section 1 we present the theoretical model, in Section 2 we present the fluidic lens prototype, in Section 3 we present experimental results for PDMS membrane characteriztion, in Sections 4 and 5 we present experimental results for fluidic lens characterization, and we demonstrate large magnification with aberrations within a fraction of the wavelength. In Section 6, we present the conclusion.

2. Theoretical model

To study the nonlinear, large deformation of a thin elastic membrane we employ the equations derived by Berger [23] for thin isotropic elastic plates:

$$\nabla^4 w - \alpha^2 \nabla^2 w = \frac{q}{D}, \tag{1}$$

$$\frac{\partial u}{\partial x} + \frac{\partial v}{\partial y} + \frac{1}{2}\left(\frac{\partial w}{\partial x}\right)^2 + \frac{1}{2}\left(\frac{\partial w}{\partial y}\right)^2 = \frac{\alpha^2 h^2}{12}. \tag{2}$$

In these equations $w(x, y)$ is the local z-displacement of the membrane, with non-deformed state corresponding to the $z = 0$ plane, $u(x, y)$ and $v(x, y)$ are the local x and y displacements, D the membrane bending rigidity, and h its thickness. The magnitude q corresponds to the applied z-load, and α is a constant to be determined from the same equations by imposing appropriate boundary conditions. Using the method of Mazumdar [24] it is possible to obtain an ordinary differential equation for w if the expression of the contour lines of equal deflection, $\psi(x, y)$, is known. In that case one integrates Eq. (1) over the area S_ψ enclosed by the contour line corresponding to a given value of ψ. Since by definition $w = w(\psi)$, one obtains from Eq. (1), for the case of uniform load q,

OSA CONTINUUM

$$\begin{aligned}\frac{q}{D}S_\psi &= \frac{d^3w}{d\psi^3}\oint_\psi \left(\psi_x^2+\psi_y^2\right)^2\frac{|dx|}{|\psi_y|}+\frac{d^2w}{d\psi^2}\oint_\psi\left[\left(\psi_x^2+\psi_y^2\right)\nabla^2\psi\right.\\ &\quad\left.+2\left(\psi_x^2\psi_{xx}+2\psi_x\psi_y\psi_{xy}+\psi_y^2\psi_{yy}\right)\right]\frac{|dx|}{|\psi_y|}\\ &\quad+\frac{dw}{d\psi}\oint_\psi\left(\psi_x\nabla^2\psi_x+\psi_y\nabla^2\psi_y\right)\frac{|dx|}{|\psi_y|}\\ &\quad-\alpha^2\frac{dw}{d\psi}\oint_\psi\left(\psi_x^2+\psi_y^2\right)\frac{|dx|}{|\psi_y|},\end{aligned}\tag{3}$$

where x and y subindexes represent partial derivatives with respect to the corresponding variable.

It is convenient to assign the value $\psi = 0$ to the boundary of the membrane, so that a boundary condition is $w(0) = 0$. For the case of a clamped membrane, another condition is $dw/d\psi = 0$ at $\psi = 0$. Since the differential equation is of third order an additional condition is required, which results generally from considerations of regularity of the solution.

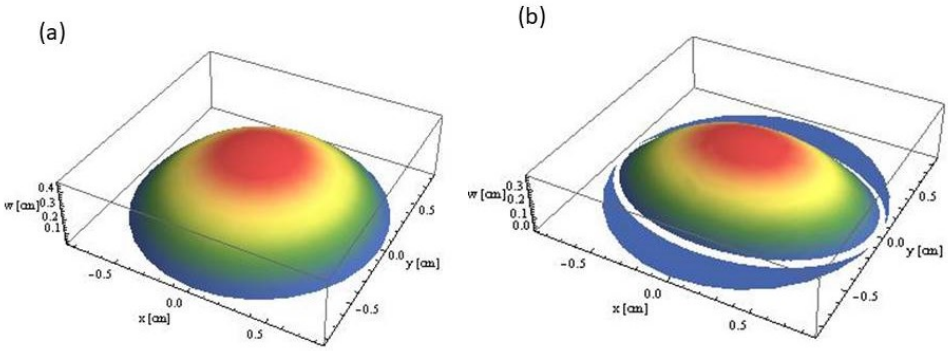

Fig. 1. Lens profile profile according to the theoretical model for a single elastic membrane for the cases: (a) circular aperture of diameter 17 mm, and (b) elliptical aperture of axes 17 mm and 12 mm. This figure was made by using Wolfram Mathematica.

On the other hand, Eq. (2) can be written, for the case of no pre-stretching ($u = v = 0$ at the clamped edge of the membrane), as

$$\frac{\alpha^2h^2}{6}S_0 = \int_0^1 d\psi\left(\frac{dw}{d\psi}\right)^2\oint_\psi\left(\psi_x^2+\psi_y^2\right)\frac{|dx|}{|\psi_y|}.\tag{4}$$

The method considered requires to know the expression of $\psi(x, y)$. In the case of an elliptical membrane of x, y semi-axes a and b, such an expression can be obtained considering that for uniform load equal deflection contour lines are expected to follow the shape of the membrane boundary at $\psi = 0$ and thus correspond to the ellipses:

$$\psi(x, y) = 1 - x^2/a^2 - y^2/b^2.\tag{5}$$

OSA CONTINUUM

Use of Eq. (5) in Eq. (3) results in

$$(\psi - 1)\frac{d^3w}{d\psi^3} + 2\frac{d^2w}{d\psi^2} + \gamma^2\frac{dw}{d\psi} = Q, \tag{6}$$

where

$$\gamma^2 = \alpha^2\frac{a^2b^2\left(a^2+b^2\right)}{3a^4+2a^2b^2+3b^4}, \tag{7}$$

$$Q = \frac{a^4b^4}{3a^4+2a^2b^2+3b^4}\frac{q}{2D}. \tag{8}$$

The solution of Eq. (6) with boundary conditions $w = dw/d\psi = 0$ at $\psi = 0$ is easily obtained changing to the variable [26]

$$\varsigma^2 = 1 - \psi, \tag{9}$$

resulting in

$$w(\varsigma) = \frac{Q}{\gamma^3 I_1(2\gamma)}\left[\gamma\left(1-\varsigma^2\right)I_1(2\gamma) + I_0(2\gamma\varsigma) - I_0(2\gamma)\right], \tag{10}$$

where I_n is the order n modified Bessel function of the first kind. In the determination of Eq. (10) the condition of finite values of w at $\varsigma = 0$ was also employed. The value of γ is determined, from the Eqs. (4), (5) and (7), as the solution to the relation

$$\gamma^2 = \frac{6}{h^2}\frac{\left(a^2+b^2\right)^2}{3a^4+2a^2b^2+3b^4}\int_0^1\left(\frac{dw}{d\varsigma}\right)^2\varsigma d\varsigma. \tag{11}$$

A plot of the lens profiles derived from the theoretical model are presented in Fig. 1 for (a) circular aperture of diameter 17 mm, and (b) elliptical aperture of axis 17 mm and 12 mm.

3. Fluidic lens prototype

The lens consists of two layers of elastic membrane of the polydimethylsiloxane (PDMS) type. The fabrication is straightforward since it is possible to use a master mold able to repeat the procedure with precision of 0.1 um to 10 nm fidelity [25]. By choosing a different thickness for the elastic membranes we can manufacture plano-convex lenses [Fig. 2(a)] or bi-convex lenses [Fig. 2(b)]. For the plano-convex case one of the membranes is made significantly thicker than the other, in order to remain uncurved under pressure. Typical thickness for the thick membrane is 1200 μm, and for the thin membrane 200 μm. The two elastic films are held together by an aluminum frame, sealed with the elastic membrane. A fluid with refractive index matched to the polymer ($n = 1.47$), such as glycerol, is injected between the elastic layers. By increasing or decreasing the fluid volume mechanically injected, it is possible to tune the focal distance across several cm, and adjust the optical power of the lens. Due to the lightness of all the components employed the overall weight of the prototype (without the frame) is less than 2 g. Further, we tune one additional degree of freedom, given by the shape of the aperture [Fig. 2(c) and 2(d)]. By modifying the aperture shape from circular [Fig. 2(c)] to elliptical [Fig. 2(d)] we can introduce different optical corrections. Typical size for the circular lens is given by a diameter d=17mm, the elliptic lenses have a mayor axis $a = 17$ mm, and minor axes $b = 15, 13$ and 12 mm. Using the theoretical model for the deformation in the elastic membrane as a function of the liquid volume, we simulated the expected focal distances of the fluidic lenses as a function of volume (Fig. 6). The focal distance range is 1cm-4cm. Using the standard conversion (1000mm/D=f), we obtain and optical power range of +25D to +100D, clearly demonstrating that our prototype operates on a larger dynamic range, not explored in previous fluidic lens designs.

In order to characterize the PDMS elastic membrane and the fluidic lens prototype we performed a number of experimental tests, as described below.

OSA CONTINUUM

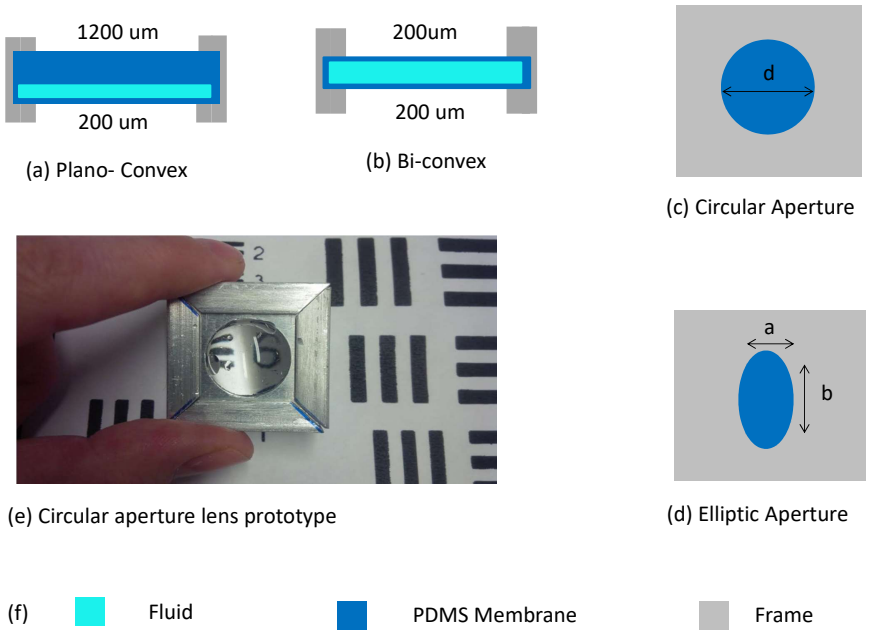

Fig. 2. Scheme of fluidic lenses. By tuning the width of the elastic membrane it is possible to design (a) planar-convex and (b) bi-convex lenses. By changing the shape of the aperture between (c) spheric or (d) elliptical, it is possible to address different visual aberrations. (e) Photograph of circular aperture lens prototype exhibiting large dioptric power. (f) Color labels.

4. Experimental results: PDMS membrane characterization

4.1. Sprectral properties

We measured the transmission spectrum of the elastic PDMS membrane, by illuminating the membrame with a stabilized broad-band Halogen Lamp (Model Thorlabs SLS201L). The transmitted spectrum was measured with a compact spectrometer (Thorlabs CCS100), with spectral range 350nm-700nm. The measured spectrum is displayed in Fig. 3. As can be observed the membrane is transparent inthe full specturm, and the absolute transmission is above 80 % for all wavelengths as required for optical, medical, and machine vision applicaitons.

4.2. Response time

For aplications requiring low latency, such as virtual or augmented reality, it is crucial to ensure a fast response in the elastic membrane. Typical brain signal are transmitted within 50 ms, therefore low latency requires reaction times shorter than this limit. To measure the response time of the membrane, we use a pin-hole and we focus the light transmitted by the lens in a photo-diode. We then press the elastic membrane and record the signal in a fast osciloscope (Rigol DG5000). By measuring the rise time in the step signal obtained, we can estimate the response time to be 43 ms (Fig. 4).

OSA CONTINUUM

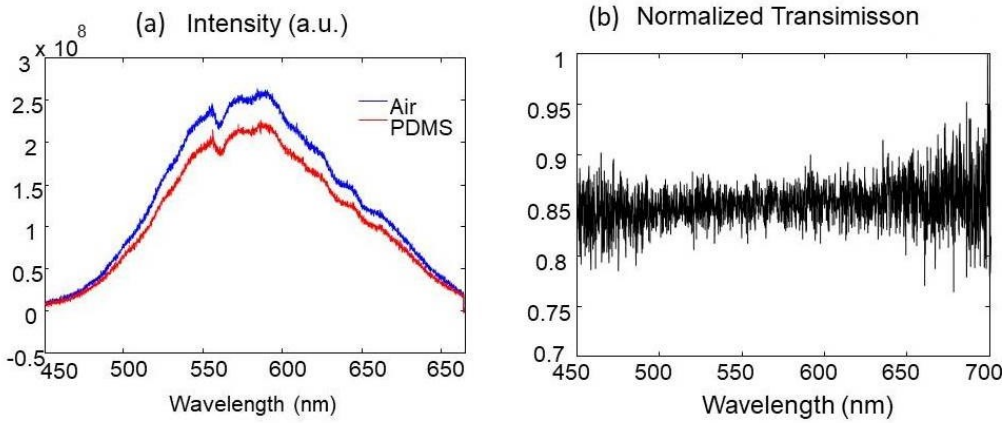

Fig. 3. Transmission spectrum of PDMS membrane obtained by iluminating the elastic membrane with an compact stabilized broad-band Halogen Lamp (Model Thorlabs SLS201L), and measuring the transmitted spectrum with a compact spectrometer (Thorlabs CCS100), in the spectral range 350nm-700nm. The figure reveals that appart from attenuation losses the membrane is transparent in the visible region.

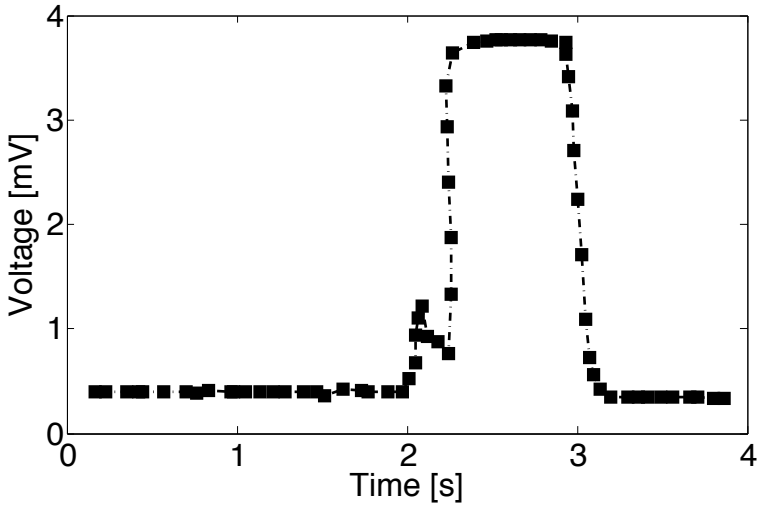

Fig. 4. Measured response time using a fast oscilloscope (Model Rigol DG500). Typical values are within 43 ms, making them suitable for low-latency applications.

5. Experimental results: fluidic lens characterization

5.1. Diffraction limit

Applications of tunable fluidic lenses in electronic wearbale devices can make use of pixalated micro-panels to project images. In such cases, diffraction through pixels in the micro-screen can play a deleterious effect. This effect can be mitigated if the optical lenses used are diffraction limited. To test this, we examined the size of the beam under focussing conditions. To this end

OSA CONTINUUM

a He-Ne beam was expanded to a typical FWHM of 645 um. The beam was sent through the macroscopid fluidic lens with spherical aperture of 17mm diameter. The focussed spot was imaged on a CCD camera (Pixel Link PLA741, pixel size 6.45 um). ND filter were used in order to attenuate the laser intensity. Images of expanded beam instensiy profiles and focused be beam intensity profiles are displayed in Fig. 5(a) and 5(b), respectively. The focussed beam spot size (FWHM) is approximately 323um. In order to determine how far this figure is from the diffraction limit, we use the Franhoufer diffraction limit (d) formula [27]:

$$d = 2.44\lambda\frac{f}{D}, \tag{12}$$

where $\lambda = 0.633\ \mu m$ is the He-Ne wavelength, $f = 20$ mm is the focal distance of the fluidic lens and the limiting apperture $D = 645\ \mu$m is the FWHM of the expanded laser beam, which is much smaller than the lens apperture itself, of diameter 17mm. The diffraction limit results in $\approx 47\ \mu$m, which is aproximatly X7 smaller than the spot size we measure. The difference could originate from non-uniformity in the PDMS membrane which can modify the membrane profile and degrade the image [22]. Higher image quality can be obtained by further controlling the properties of the membrane upon fabrication.

5.2. Resolving power

We tested the resolving power of the fludic lenses by probing the lenses against calibrated optical targets of the type Edmund Optics 1951 USAF Hi-Resolution Target. A resolution target was set at approximately 3 cm distance from the fluidic lens, and photos were taken with a webcam. For the case of the spherical lens, we found that it is typicall capable of resolving more than 10 line-pairs/mm (Fig. 6), this number can be further increased by increasing the fluid volume and thus the optical power. For the eliptic aperture lenses, we found the resolving power to be slightly lower, typically of order 5 line-pairs/mm, due to the optical aberrations induce by the lens. This resolving power was also confirmed by the far field diffraction pattern of a calibrated slit. The high resolution of the lenses make the suitable for professional applications where razor-sharp resolution is required, such as in surgery or other medical applications.

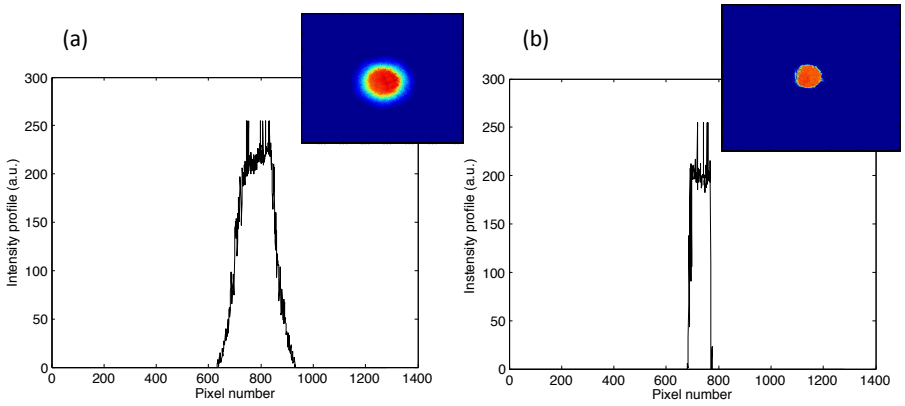

Fig. 5. (a) Intensity probfile for an expanded beam, (b) intensity profile for a focused beam through a fluidic lens of focal distance 20mm.

OSA CONTINUUM

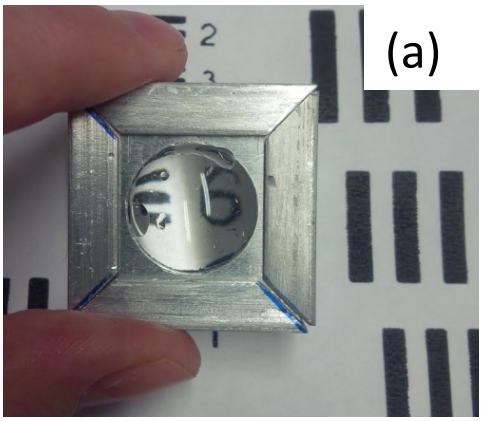

Fig. 6. Resolution power tested via calibrated targets. (a) Spherical lens has a resultion of at least 10 line-pairs/mm. These figures can be increased by increasing the fluid volume, making the fluidic lenses suitable for razor-sharp professional applications.

5.3. Focal distance

Tunable optical power is a very desirable property for any user-oriented device. In particular, for eye-wear lenses, cameras or other machine vision applications. One main application is for instance in correcting for presbyopia. Typical multi-focal crystal lenses, are static and can only contain a limited number of focal distances, making the field-of-view of the lens itself very narrow. The tunable lens we demonstrate here can provide for a continuum of focal distances expanding across several cm without compromising the field-of-view. In order to characterize the focusing properties of the fabricated adaptive lenses, we use an expanded He-Ne laser (Melles-Griot 05-LHR-111, λ = 633 nm) providing a collimated beam after transmission through a collimator, see experimental scheme in Fig. 7(a).

We measured the effective position (f) of focusing spot using a photo-diode mounted on a translation stage. In this way we can identify the effective focal distance by maximazing the voltage measured on the photo-diode. We also verify this measurement visually, using a moving millimetric screen. We measured the focus dynamic range of the fabricated prototype by increasing the fluidic volume from an initial arbitrary value V_0. In our demonstration we increased the fluidic volume mechanically in steps of 1 ml, however this volume can alternatively be controlled via voltage, motors, or electronic means. The measured dynamic range is displayed in Fig. 8, and is larger than 3 cm, expanding the region from 33D to 66D. We measured the optical power of the lenses, for the case of circular aperture and elliptic aperture. By changing the fluidic volume the optical power and focal distance can be tuned in the expected range, as predicted by the mode (Fig 8).

In order to further characterize the light field produced by the fluidic lenses, we reconstructed the wave-front transmitted through the lenses using a Shack-Hartmann wave-front sensor [Model Thorlabs WFS150-5C, see Fig. 7(b)]. To this end, we used a collimated incoherent LED source (λ = 633 nm). The incident field had a residual field curvature below $\lambda/6$. The sensor was placed 2 cm apart from the fluidic lens, in order to reconstruct the central region of the near field, with an aperture limited by the pupil size of the sensor itself, typically 3mm diameter. We reconstructed the wave-front produced by a circular fluidic lens filled with V_{max} = 6 ml corresponding to an optical power (OP)= 50D [Fig. 3(a)], and by an elliptical fluidic lens filled with V_{min} = 4 ml corresponding to OP=36D. The qualitative difference in the wave-front due to the shape of the aperture is apparent. Furthermore, for lenses filled with V_{min} we encountered larger deformations

OSA CONTINUUM

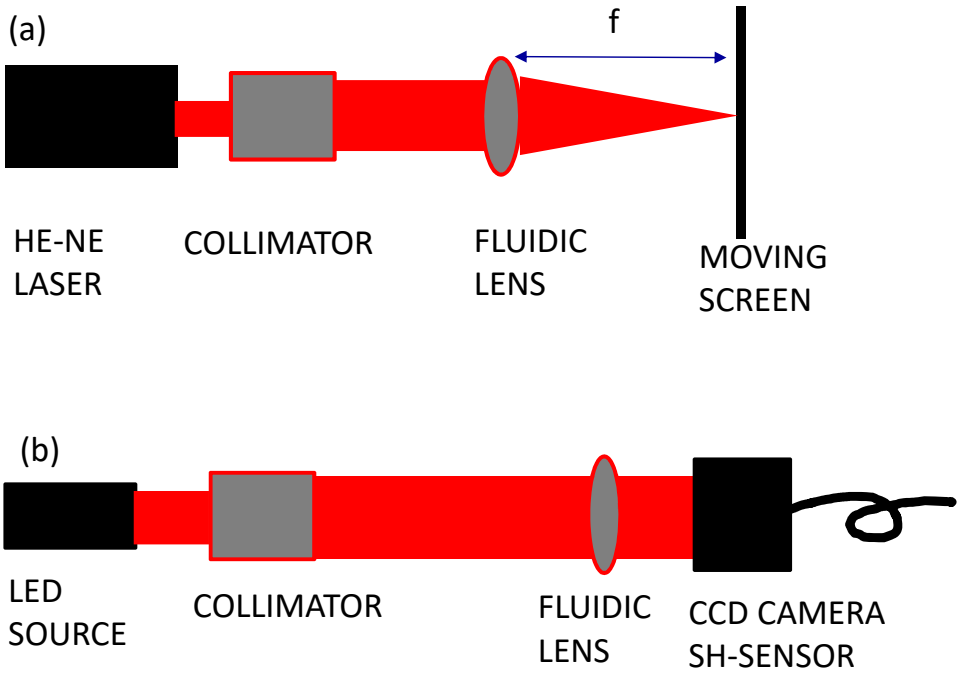

Fig. 7. (a) Experimental scheme for measuring the focal distance of the fluidic lenses using a He-Ne laser source (Melles Griot 05-LHR-111, λ = 633 nm). (b) Experimental scheme for reconstruction of wave-front produced by fluidic lenses and characterization of optical aberration, using a LED source (λ = 633nm) and a Shack-Hartmann wave-front sensor (Thorlabs WFS150-5C).

in the wave-front, due to the fact that the membrane was subjeted to a lower tension regime (Fig. 9).

6. Lens aberration measurements

In order to experimentally characterize the optical aberrations of the central region of the fluidic lens prototype, we use the experimental setup described in Fig. 7(b). A collimated incoherent beam, produced by a LED source (λ = 633 nm) propagates through the fludic lens and is imaged by a Schack-Hartmann wave-front sensor (Model Thorlabs WFS150-5C), located at a distance of 2 cm from the fluidic lens, in order to image the near field produced by the lens. The area of the beam to be characterized is determined by the aperture of the sensor (typically 3mm). We measured the aberrations in μm, in terms of the coefficients associated with Zernike polynomials up to 4th order ($Z_{2,-2}$, $Z_{2,2}$, $Z_{3,-3}$, $Z_{3,-1}$, $Z_{3,1}$, $Z_{3,3}$, $Z_{4,-4}$, $Z_{4,-2}$, $Z_{4,0}$, $Z_{4,2}$, $Z_{4,4}$), corresponding to trefoil(X,Y), astigmatism(X,Y), spherical, and coma. The first three orders are not displayed since they correspond to a constant term and an arbitrary linear tilt. The Zernike coefficients were measured for two different fluidic volumens and optical powers (OP) given by V_{max} = 6 ml, OP=50 D (Fig. 5 left colum) and V_{min} = 4ml, OP= 36 D (Fig. 5 right column). In Fig. 10, we show the experimental results for wave-front reconstruction in terms of Zernike polynomials for fluidic lenses with three different apertures. Figure 10(a) circular aperture d = 17 mm, Fig.

OSA CONTINUUM

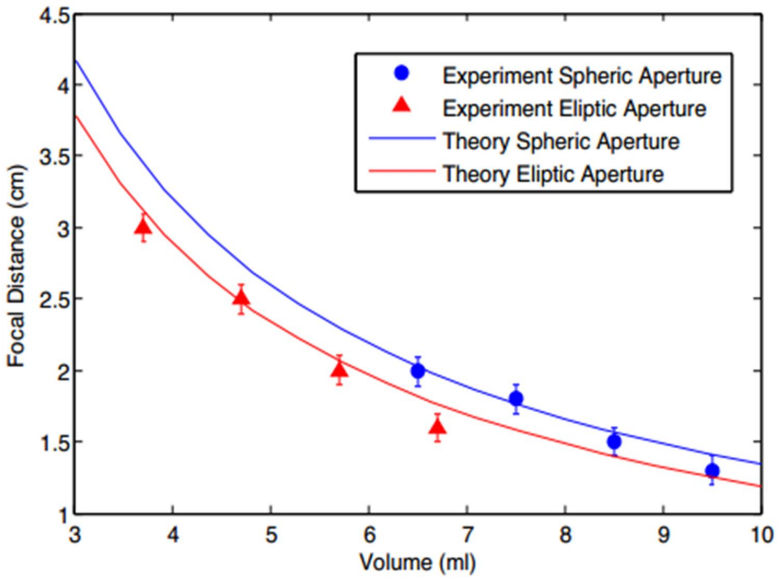

Fig. 8. Measured focal distance vs. fluidic volume for a lens with elliptic aperture (red triangles) and circular aperture (blue circles). Blue curve: Theoretical prediction for a spheric lens with 17mm diameter. Red curve: Theoretical prediction for an elliptic lens with mayor and minor axes 17 mm and 15 mm, respectively. Measured Optical Power (OP) dynamic range: 33D to 66D. The agreement between experiment and theory is apparent.

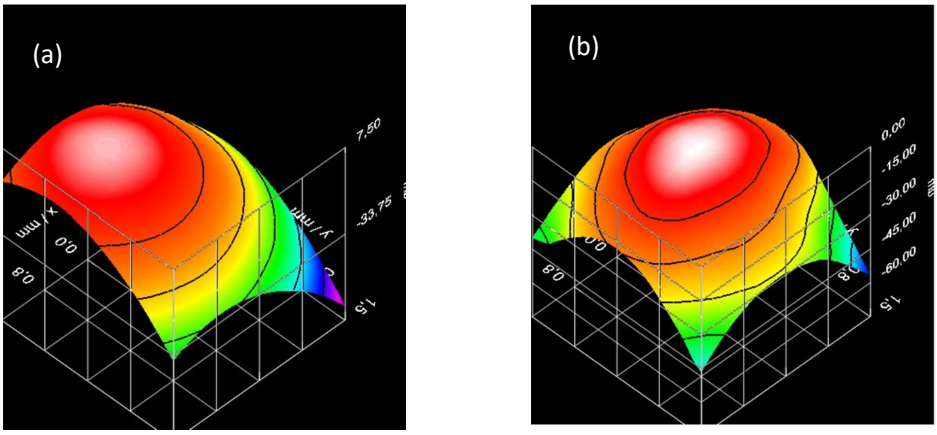

Fig. 9. Wave-front reconstruction using wave-front sensor (Thorlabs WFS150-5C) for a fluidic lens with (a) spheric aperture, (b) elliptic aperture.

10(b) elliptic aperture mayor axis $a = 17$ mm and minor axis $b = 15$ mm, Fig. 10(c) elliptic aperture with mayor axis $a = 17$ mm minor axis $b = 13$ mm. In all cases the aberrations are within a fraction of the wave-length. The larger number of aberration measured for the case of small fluidic volume is ascribed to the lower tension regime on the elastic membrane.

For completeness, we contrasted the experimental results with a simple theoretical model

OSA CONTINUUM

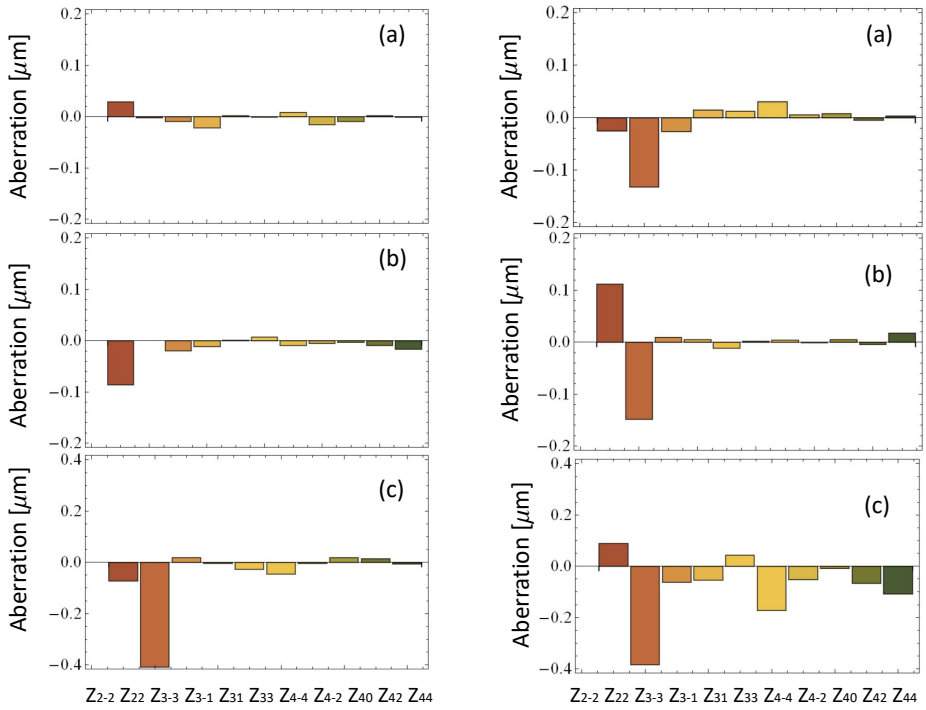

Fig. 10. Measured typical aberrations (trefoil(X,Y), astigmatism(X,Y), spherical, and coma) in μm, in terms of Zernike polynomial ($Z_{n,m}$) coefficients up to 4th order. Left column corresponds to V_{max} = 6 ml (OP=50D), right column corresponds to V_{min} = 4 ml (OP=36D). (a) Circular aperture (d = 17 mm), (b) elliptic aperture (axes a = 17 mm, b = 15mm), (c) elliptic aperture (axes a = 17 mm, b = 13mm). Typical aberrations are within a fraction of the wavelength λ = 633 nm.

based on the effects of a single elastic membrane, which quantifies the phase difference for a wave-front propagation along a distance $z = d$ with respect to ϕ_0 at $z = 0$, based on the equation $\phi_d = \phi_0 + \frac{2\pi}{\lambda}\left[n_f w(x,y) + \frac{d - w(x,y)}{k_{rz}}\right]$, with $k_{rz} = \frac{n_f\left(w_x^2+w_y^2\right)+\sqrt{1+\left(1-n_f^2\right)\left(w_x^2+w_y^2\right)}}{1+w_x^2+w_y^2}$. Theoretical results confirm that in all cases optical aberrations are below a fraction of the wavelength λ, in good agreement with experimental results. We note this model does not account for the effect of the two membranes or the effect of gravity.

7. Conclusions

We have reported on the design, fabrication, and characterization of macroscopic fluidic lenses with high dioptric power, tunable focal distance and aperture shape. An experimental analysis of the lens aberrations demonstrate that optical aberrations are within a fraction of the wavelength. In addition the lenses are extremely light and affordable. We argue all of this indicates the proposed prototype is highly suitable for the low vision segment, as well as for camera, optical zooms, microscope objetctives, and other machine vision applications where large magnification can be required.

OSA CONTINUUM

Funding

Agencia Nacional de Promoción Científíca y Tecnológica (PICT2014-1543, PICT2015-0710 Startup, UBACyT PDE 2016, UBACyT PDE 2017).

Acknowledgments

The authors are grateful to the Solar Energy Department (TANDAR-CNEA) and to the Laboratory of Polymers (FCEN-UBA) for assistance in PDMS membrane preparation. GP gratefully acknowledges financial support from PICT2014-1543, PICT2015-0710 Startup, UBACyT PDE 2016, UBACyT PDE 2017. The authors are thankful to Stephan Baumer for many fruitful discussions.

References

1. D. A. Goss and R. W. West, *Introduction to the Optics of the Eye* (Butterworth-Hienemann, 2001).
2. M. P. Keating, Geometric, *Physical and Visual Optics* (Butterworth-Hienemann, 2002).
3. W. Tasman and E. A. Jaeger, *Duane's Ophtalmology* (LLW, 2013).
4. T. Callina and T. P. Reynolds, "Traditional methods for the treatment of presbyopia: spectacles, contact lenses, bifocal contact lenses," Ophthalmol. Clin. North Am. **19**, 25–33 (2006).
5. Y. Lo and D. Zhang, "Fluidic adaptive lens," WO patent application WO2006011937A2 (February 2, 2006).
6. N. Hazan, A. Banerjee, H. Kim, and C. Mastrangelo, "Tunable-focus lens for adaptive eyeglasses," Opt. Express **25**, 1221–1233 (2017).
7. N. Hasan, M. Karkhanis, C. Ghosh, F. Khan, T. Ghosh, H. Kim, and C. H. Mastrangelo, "Lightweight smart autofocusing eyeglasses," Proc. SPIE **10545**, 1054507 (2018).
8. G. Puentes, D. Voigt, A. Aiello and J. P. Woerdman, "Experimental observation of depolarized light scattering," Opt. Lett. **30**, 3216–3219 (2005).
9. G. Puentes and F. Minotti, "Melt supply equipment, casting apparatus and casting method," KR patent application 20170102760 (September 12, 2017).
10. K. Wei, H. Huang, Q. Wang, and Y. Zhao, "Focus-tunable liquid lens with an aspherical membrane for improved central and peripheral resolutions at high diopters," Opt. Express **24**, 3929–3939 (2016).
11. P. Zhao, Ç. Ataman, and H. Zappe, "Spherical aberration free liquid-filled tunable lens with variable thickness membrane," Opt. Express **23**, 21264–21278 (2015).
12. M. Vallet, B. Berge, and L. Vovelle, "Electrowetting of water and aqueos solutions on poly-ethilene-terephthalate insulating films," Polymer **37**, 2465–2470 (1996).
13. T. Krupenking, S. Yang, P. Mach, "Tunable liquid microlens," Appl. Phys. Lett. **82**, 316–318 (2003).
14. S. Kuiper and B. H. Hendriks, "Variable-focus liquid lens for miniature cameras," Appl. Phys. Lett. **85**, 1128–1130 (2004).
15. G. C. Knollman, J. L. Bellini, and J. L. Weaver, "Variable-focus liquid-filled hydroacoustic lens," J. Acoust. Soc. Am. **49**, 253–261 (1971).
16. N. Sigiura and S. Morita, "Variable-docus liquid-filled optics lens," Appl. Opt. **32**, 4181–4186 (1993).
17. D. Y. Zhang, V. Lien, Y. Berdichevsky, J. Choi, and Y. H. Lo, "Fluidic adaptivelens with high focal length tenability," App. Phys. Lett. **82**, 3171–3172 (2003).
18. K. H. Joeng, G. L. Liu, N. Chronis, And L. P. Lee, "Tunable microdoublets lens array," Opt. Express **12**, 2494–2500 (2004).
19. J. Chen, W. Wang, J. Fang, and K. Varahramyan, "Variable focusing microlens with microfluidic chip," J. Micromech. Microeng. **14**, 675–680 (2004).
20. N. Chronis, G. L. Liu, K. H. Jeong, and L. P. Lee, "Tunable liquid filled micro-lens array integrated with microfludidic network," Opt. Express **11**, 2370–2378 (2003).
21. P. M. Moran, s. Dharmatilleke, A. H. Khaw, and K. W. Tan, "Fluid lenses with variable focal length," App. Phys. Lett. **88**, 041120 (2006).
22. H. Ren and S.-T. Wu, "Variable-focus liquid lens," Opt. Express **15**, 5931–5936 (2007).
23. H. M. Beger, "A new approach to the analysis of large deflections of plates," J. Appl. Mech. **22**, 465–472 (1955).
24. J. Mazumdar, "A method for solving problems of elastic plates of arbitrary shape," J. Aust. Math. Soc. **11**, 95–112 (1970).
25. N. A. Polson and M. A. Hayes, "Microfluidics controllling fluids in small places," Anal. Chem. **73**, 312A–319A (2001).
26. J. Mazumdar and R. Jones, "A simplified approach to the analysis of large deflections of plates," J. Appl. Mech. **41**, 523-524 (1974).
27. E. Hetch, *Optics,* 2nd ed. (Addison Wesley, 2002).